Fifth International Conference on CFD in the Process Industries
CSIRO, Melbourne, Australia
13-15 December 2006

NUMERICAL ANALYSIS OF GAS FLOW-SLAG SURFACE INTERACTION IN BLAST FURNACE

Baoyu GUO[1], Paul ZULLI[2], Daniel MALDONADO[2] and Aibing YU[1]

[1]Centre for Simulation and Modelling of Particulate Systems, School of Materials Science and Engineering, University of New South Wales, Sydney, NSW 2052, Australia

[2]Bluescope Steel Research, P.O. Box 202, Port Kembla, NSW 2505, Australia

ABSTRACT

An improved understanding of gas flow distribution around the raceway of an ironmaking blast furnace is important for stable operation and improved drainage of molten liquids from the hearth. Previous studies based on 2- and 3-dimensional models with over-simplified raceway phenomena do not provide a quantitative description of liquid-gas interaction. The current paper focuses on the analysis of gas flow near the raceway region and its effect on the liquid surface by using a 3-dimensional sector model. Various BF phenomena and a realistic local coke bed structure, such as the raceway cavity and "birds nest", are considered. The simulation is conducted using a homogeneous two-phase flow model combined with a model for flow through porous media. The variables considered include the liquid level, location and shape of the cohesive zone and deadman characteristics.

INTRODUCTION

The gas flow distribution around the raceway of an ironmaking blast furnace (BF) is complex due to its asymmetry, the non-uniformity of the packed bed and transient behaviour of the molten liquids removed during each tapping cycle. Improved understanding of the gas and liquid flow in this region is important for stable operation and improved drainage or removal of molten liquids from the hearth. High temperature, gaseous conditions in the lower zone make direct measurements within the furnace difficult, hence, use of numerical simulation based on fluid dynamics, reaction kinetics, etc is a useful tool in obtaining insights into complicated in-furnace phenomena. This is usually carried out through parametric studies.

Several different approaches to numerical modelling of the blast furnace have been explored. Some of these models simplified the problem by using 2-dimensional (2-D) slot or symmetry (Dong et al., 2006; Chew et al., 2001). These assumptions do not adequately take account of the divergence of the gas flow exiting the tuyeres (ie the ports for the hot blast), let alone the complex coke bed structure in the raceway region. In some of the models developed to simulate conditions in the BF shaft (Mondal et al., 2005; Nogami et al., 2004a), the blast inlet was typically assumed as azimuthally uniform through a circumferential slot of uniform width. As such, a 3-dimensional (3-D) model can provide more precise information for simulating flows in the BF lower zone, due to the discrete nature of the tuyeres and tapholes, and localized raceway boundary structure. In fact, some 3-D process models have been attempted to study the overall behaviour of the upper section of the furnace (e.g., Castro et al., 2002), but the coarse grids used prevent accurate resolution of the complex flow patterns near the raceway. These simplifications will most likely provide inaccurate predictions of the gas flow distribution. Moreover, these models rarely consider the effect of the important raceway phenomena, such as the impact of coke fines generated within the raceway on coke bed permeability.

Regarding previous numerical models of the hearth, nearly all the experimental and numerical studies on the BF liquids drainage were carried out without considering the effect of gas flow on the free (slag) surface (Pinczewski and Tanzil, 1981; Nishioka et al., 2005). The free surface is important for liquid tapping operations, since the liquid residual after each tapping cycle is closely related to the shape of the free surface. In some BF operations, a phenomenon called the "splashy stream" is observed, where the furnace gas is expelled prematurely during liquids drainage, contributing to taphole and refractory wear (He et al., 2002). It is unknown whether the short-circuiting of furnace gases is due to dynamics of free liquid surface or the formation of viscous fingers (see Tanzil, 1985), but it is apparently related to the liquid surface behaviour.

From the above, there is an obvious gap in knowledge concerning the gas flow distribution and extent of gas-liquid interaction in the BF lower zone at or below the raceway region. This is the main motivation for the current work, which aims to simulate gas flow under realistic geometric and boundary conditions, and consequently, to understand the effect of various operational scenarios on the gas flow and liquid surface. The effect of various parameters, including raceway fines, liquid surface level, cohesive zone type/location, deadman porosity/surface profile, are considered systematically.

MODEL DESCRIPTION

The gas-liquid problem here is considered as a continuous flow through porous media with a free surface, with the mean void velocities and pressure distribution calculated by using a so-called homogeneous model. The homogeneous model is a simplification of the multi-fluid model. It assumes the same velocity for all phases but uses distinct volume fractions, r_α, for each phase α. The set of steady state fluid flow governing equations are as follows (NB Turbulence is not considered):

Continuity equation

$$\frac{\partial}{\partial t}(\varepsilon r_\alpha \rho_\alpha) + \nabla \cdot (\varepsilon r_\alpha \rho_\alpha \mathbf{u}) = 0 \tag{1}$$

Momentum equation

$$\frac{\partial}{\partial t}(\varepsilon \rho \mathbf{u}) + \nabla \cdot (\varepsilon \rho \mathbf{u}\mathbf{u}) - \nabla \cdot (\mu \varepsilon (\nabla \mathbf{u} + (\nabla \mathbf{u})^T)) = \varepsilon \mathbf{g} - \varepsilon \nabla p - \varepsilon R_0 \mathbf{u} \tag{2}$$

where ε denotes porosity. The density and viscosity in Eq (2) are given as follows:

$$\rho = \sum_{\alpha=1}^{N_P} r_\alpha \rho_\alpha \;, \mu = \sum_{\alpha=1}^{N_P} r_\alpha \mu_\alpha \tag{3}$$

where N_P is the total number of phases. This is equivalent to single phase flow with variable density and diffusivity. The resistance coefficient R_0 is calculated according to the Ergun equation. ANSYS-CFX4.4 solver was used for the calculation.

MODEL VALIDATION

The model was initially compared with experimental results from a 2-D drainage model (Pinczewski and Tanzil (1981)). The simulated results are compared with measurements in terms of the temporal evolution of the free surface (Figure 1). Good agreement between these results indicates that the model performs well for such a free surface flow through packed bed.

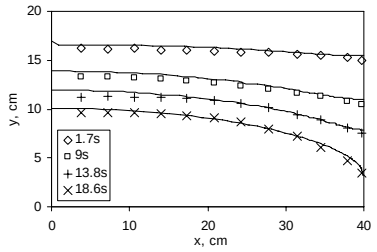

Figure 1: Comparion of computed (solid line) and experimental (symbol) free surface profiles, after Pinczewski and Tanzil (1981).

BOUNDARY CONDITIONS AND FLUID PROPERTIES

The two phases considered, i.e., gas and liquid slag are assumed to be incompressible, for simplicity, with constant physical properties. Practically the gas density is related to pressure, temperature and compositions. The density of the gas is set as 0.8 kg/m^3 and its viscosity is 5.4×10^{-5} Pa s, which are typical of the gas properties in the raceway zone. The density of slag is set as 2500 kg/m^3, and its viscosity is set as 0.5 Pa s.

The gas inlet flowrate for each tuyere is 10,825 Nm^3/h. This is equivalent to a velocity of 275 m/s at the tuyere nose of 150 mm ID. The flowrate of gas exiting the raceway (bosh gas) is 15,180 Nm^3/h. This difference is the gasification rate of primarily carbonaceous specifies (coke, coal) – these are simulated as a mass source uniformly generated in the raceway cavity. The mean source is calculated to be 0.225 kg/sm^3. The outlet for the gas phase at the BF top is set as a pressure reference point (constant pressure) and the pressure field relative to the BF top outlet is solved.

The main geometric dimensions are shown in Figure 2. A 1/28th scale sector corresponding to a single tuyere is considered. A 3-D block structured mesh is shown in Figure 3, with each side being set as a symmetry plane. Liquid drainage and dripping are not considered, and the lower boundary of the simulation domain is taken at roughly the taphole level. The solid coke bed is assumed stationery and only the mean interstitial velocity of fluid flow is calculated. The entire BF is divided into several distinct zones, namely, lumpy zone (LZ), cohesive zone (CZ), raceway zone (RZ), active zone (AZ) and deadman zone (DZ), with different porosity being set for each zone. The coke layer slit (or opening) is assumed to be horizontal in the cohesive zone, so that flow across the cohesive zone is directed with little permeability in the vertical direction.

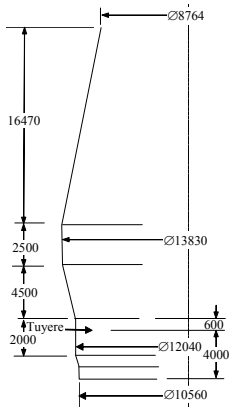

Figure 2: Model dimensions.

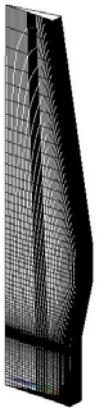

Figure 3: Computational grid

The raceway region is regarded as one of the most important zones as it influences the distribution of the gas and its composition, as well as movement of solid particles within the furnace. At the back of the raceway, fine coke and char accumulate forming a region of low permeability (referred to as the "birds nest"). This region was not only observed through BF dissection (Tate et al., 1976; ISIJ, 1987), but also predicted by CFD-DEM methods (Nogami et al., 2004b). A representative coke bed structure is considered in the current model. An oval-shaped raceway cavity is implemented with a layer of fine particles representing the 'birds nest' at the lower part of the raceway back wall. The porosity and particle size are shown in Figure 4, and are displayed directly in Figure 5. Figure 4(a) also shows two representative cohesive zone shapes, viz. 'inverted V'- and 'W'-shaped, with assumed porosity and particle size. The values of dimensions and parameters represent the base case and will be taken as default values for the parametric study, together with a liquid level of 1 m below the tuyere centre.

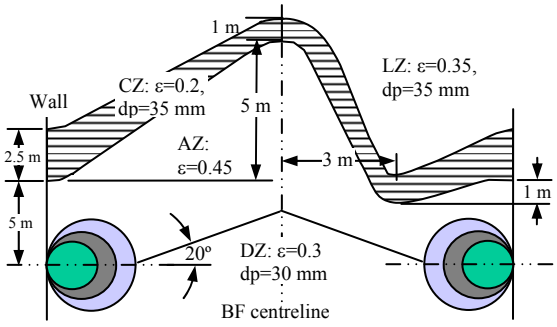

(a)

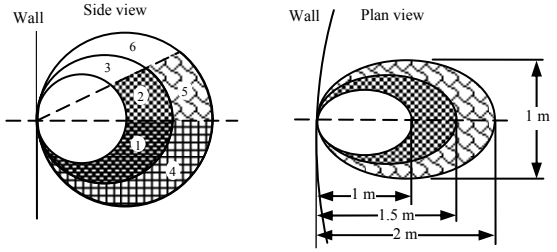

Zone	ε	d_p,mm	Permeability, mm^2
1	0.1	5	0.0002
2	0.15	10	0.0031
3	0.25	20	0.0741
4	0.15	10	0.0031
5	0.25	20	0.0741
6	0.3	30	0.3306

(b)

Figure 4: Assumed distribution for porosity and particle size for the base cases. (a) 'inverted V'- and 'W'-shaped cohesive zone, (b) Raceway zone.

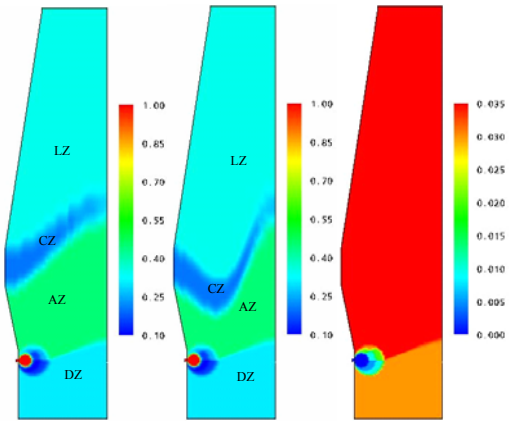

(a) (b)

Figure 5: (a) Porosity distributions for two types of cohesive zone shapes; (b) Particle size.

TYPICAL RESULTS

Gas Velocity Distribution

Although the numerical model is formulated to track the gas-liquid interface, the highly non-uniform packing structure means that computational efficiency is improved by calculating the converged velocity and pressure fields prior to moving the free surface. Figure 6 shows the gas flow streamlines (exiting the tuyere) and absolute velocity distribution contours. Figure 7 highlights the gas recirculation in the raceway cavity and the local pressure distribution. Typically, a high velocity jet from the tuyere is directed slightly upward by the 'birds nest' and is confined to the raceway cavity. The pressure is generally higher inside the cavity, particularly at the impact point of the jet on the raceway wall. The velocity decreases sharply in the 'birds nest' region due to low permeability. The velocity becomes relatively high in the central part of the active zone, where flow cross-sectional area is reduced by restriction of the neighbouring sectors. Thus this region can be understood as one where gas streams from different tuyeres emerge. The gas velocity increases through the cohesive zone due to the reduced cross sectional area.

There are three low velocity zones located at: (a) Lower side of the cohesive zone near the wall, where the wall effectively prevents horizontal gas flow; (b) Central part or apex of the cohesive zone, where vertical flow is prevented; and (c) Central region immediately above the liquid surface, where the low-permeability deadman is exposed to the gas flow.

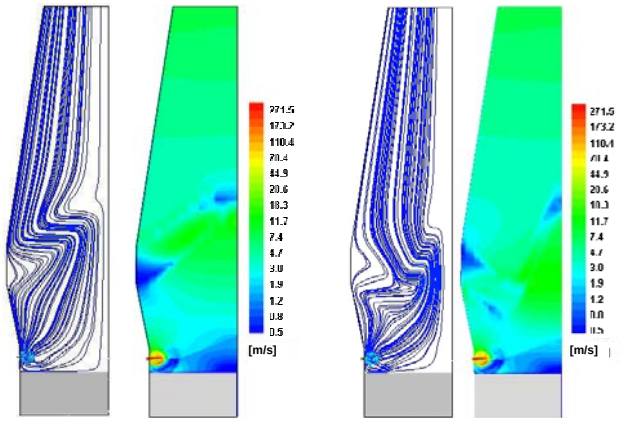

(a) (b)

Figure 6: Streamlines and velocity isopleths showing typical gas flow patterns for two shapes of cohesive zone. (a) 'inverted V'; (b) 'W'-shaped. Note liquid region is coloured in grey.

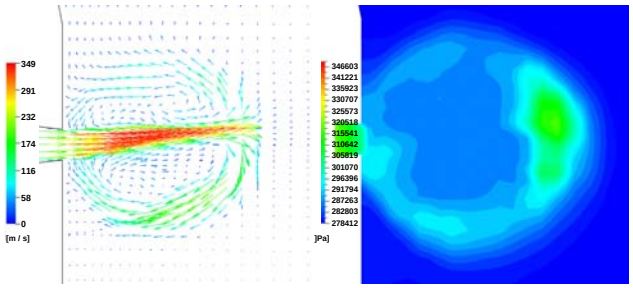

Figure 7: Gas flow and pressure distribution in the raceway, showing recirculation in the cavity.

Pressure Distribution on Liquid Surface

Due to a localized high velocity near the tuyere, pressure varies over the liquid surface. Normally, it is lower at the furnace centreline and higher at the periphery below the tuyere. Figure 8 shows a radial profile of the liquid surface pressure and Figure 9 shows the pressure distribution in the liquid phase. This pressure difference increases as liquid level increases. The magnitude of pressure difference on the liquid surface represents a driving force that would distort the initially flat liquid surface (i.e. before the start of a liquid tapping cycle) and the liquid surface during drainage. In particular, the local high pressure near the raceway will cause a depression in the liquid surface, as shown in Figure 9(b). Therefore, the pressure difference is a key dependent variable in the current study. Note that the pressure is evaluated in units, metres of slag (mSlag), for easier interpretation.

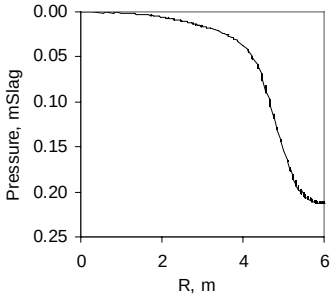

Figure 8: Radial profile of the liquid surface pressure.

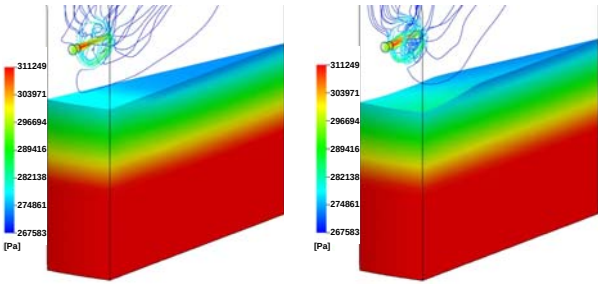

(a) (b)

Figure 9: Pressure distribution in liquid versus liquid surface shape. (a) Before deformation, (b) After deformation.

PARAMETRIC STUDY

Variables studied include the cohesive zone (CZ) shape and location, deadman profile, liquid level and gas flowrate. The effects of these variables are quantified in terms of the maximum liquid surface pressure difference (SPD), as discussed below.

Raceway Structure

The coke bed structure in the vicinity of the tuyere, such as the cavity size and fine particle layer (or 'birds nest') depth, significantly influences the pressure distribution. If the assumed birds nest with low permeability is neglected, the value of SPD drops by as much as 50%. The higher resistance across the bird nest creates a higher mean pressure within the cavity, which will increase the surface pressure below the cavity, compared with the case without birds nest.

Cohesive Zone

Typically, the root of the CZ (the wall-touching point) is located near the belly of the furnace (between the shaft and bosh), approximately 5m above the tuyere level. Two typical CZ shapes are considered, 'inverted V' and 'W' (Figure 5). The impermeability of the soft ore layer and its orientation (currently horizontal) in the cohesive zone are partially responsible for the local high pressure in the raceway. The location of the CZ, particularly near the wall, affects the local velocity distribution near the raceway and subsequently, the pressure distribution along the liquid surface. This effect is examined by a vertical translation of the entire CZ. Figure 10 shows a series of velocity contours corresponding to different 'W'-shaped CZ locations and Figure 11 shows corresponding changes in the streamline pattern. As shown in

Figure 12, for each type of profile, the value of SPD increases significantly as the CZ root approaches the tuyere level. Generally a 'W'-shaped CZ creates a higher SPD than an 'inverted V'-shaped CZ for the same CZ root level. The difference caused by the change of CZ shape depends largely on a specific CZ location. There is little difference in SPD for the base case, in which the CZ root is 5.0 m above the tuyere level. At such a long distance, the effect of the CZ on the liquid flow can be ignored. However, such an effect can be very important when the CZ is low, for example, when the CZ root is 2 m above tuyere level, where a switch from 'inverted-V' to 'W' shape can lead to a threefold increase in SPD.

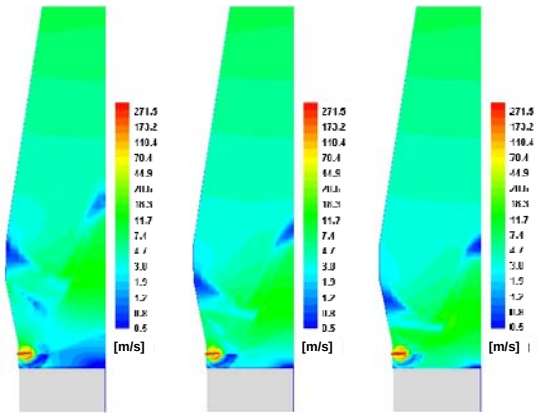

(a) (b) (c)

Figure 10: Velocity isopleths showing the effect of CZ root location (above the tuyere, in metres) for the case of a 'W'-shaped CZ. (a) 5m, (b) 3m, (c) 2m.

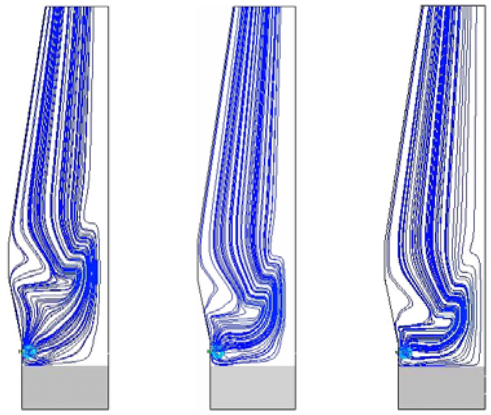

(a) (b) (c)

Figure 11: Streamlines showing the effect of cohesive zone root location (above the tuyere, in metres) for the case of a 'W'-shaped CZ. (a) 5m, (b) 3m, (c) 2m.

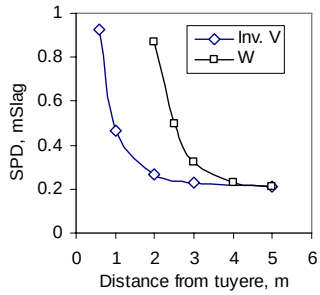

Figure 12: Liquid surface pressure difference as the function of cohesive zone root location. The legend indicates the CZ type.

Deadman

The pressure on the liquid surface may be affected by changes in the gas flow pattern when the boundary and the permeability of the deadman change, e.g. upward movement of the deadman relative to the upper liquid surface, due to higher liquid buoyancy forces.

Surface profile:

The shape or surface profile of the upper boundary of the deadman region is assumed to be conical. The effect of the deadman surface profile is examined by fixing the root position while changing the angle of repose. The SPD is found to be insensitive to the angle of repose, regardless of different deadman porosity (0.1-0.3). However, the overall pressure on the liquid surface increases with increasing angle as shown in Figure 13. This is because the interface between the deadman and the active zone (region above the deadman) moves with the angle and consequently the overall pressure drop through the BF is changed. As the angle of repose increases, the volume of the active zone (with higher porosity cf the deadman) decreases, which subsequently causes a higher gas pressure drop.

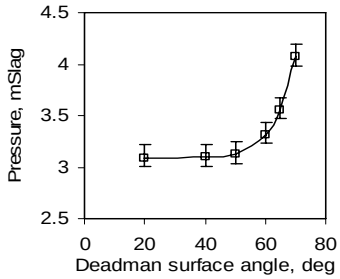

Figure 13: Effect of the angle of repose or deadman surface angle on liquid surface pressure. The solid line represents the mean surface pressure and error bars represent the range. (Liquid level is 1m below the tuyere level, 'W'-shaped CZ).

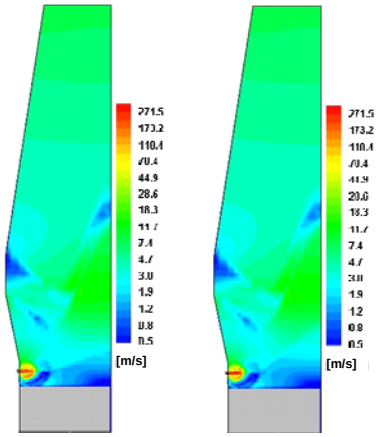

(a) (b)

Figure 14: Effect of angle of repose or deadman surface angle on velocity distributions for a 'W'-shaped CZ. (a) 20°, (b) 40°.

Porosity

A change in deadman porosity may also affect the gas flow distribution. For example, a three-fold reduction in porosity (from 0.3 to 0.1) could increase the SPD by 40% (Figure 15). As shown in Figure 16, the gas flow is restricted to the region outside the deadman, when the deadman is impermeable.

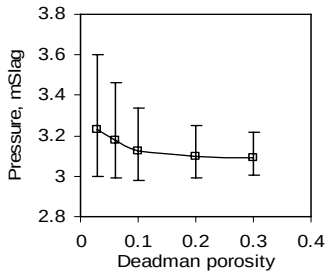

Figure 15: Effect of deadman porosity on liquid surface pressure. Curve represents the mean surface pressure and error bars represent the range.

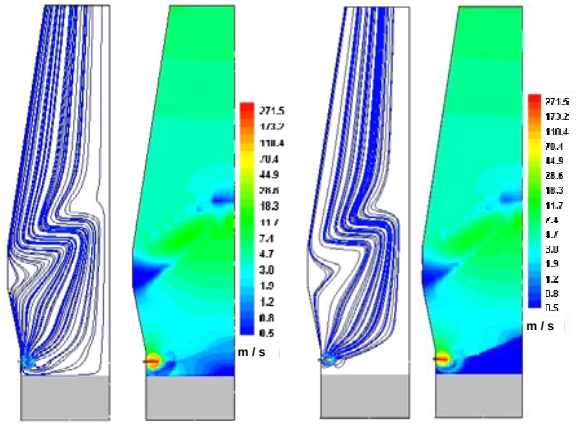

Figure 16: Gas flow distribution, showing the effect of the porosity of deadman (a) 0.3; (b) 0.1.

Liquid Surface Level

Figure 17 shows that aside from a greater deadman volume being exposed to gas flow, the gas flow distribution remains relatively unchanged with liquid level variation. Due to the gas-liquid interaction, the liquid surface pressure is slightly affected by the distance between the liquid surface and tuyere. As shown in Figure 18, it becomes smaller as the liquid level drops during drainage. Considering that the taphole is about 4.0m away from the tuyere level, it is expected that the effect of gas flow on the drainage process is very small. However, when the cohesive zone is abnormally low, the effect will become stronger.

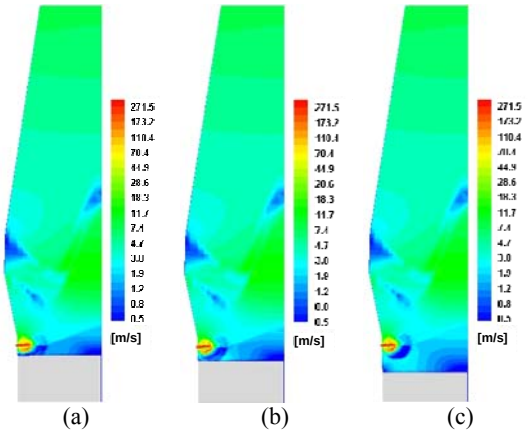

Figure 17: Gas velocity contours for different liquid levels relative to the tuyere level (colour to logarithmic scale in the range above 0.5). (a) 0.75 m; (b) 1 m; (c) 2 m.

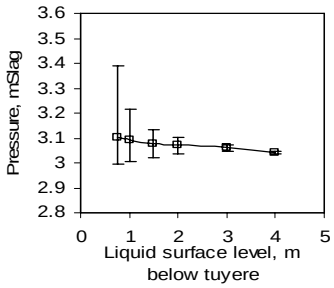

Figure 18: Effect of liquid level on the liquid surface pressure difference.

Figure 19 shows the pressure distribution on the liquid surface, for three different liquid levels. When the liquid level is high, a localized high-pressure region appears below each individual raceway. As the liquid surface descends, these high pressure regions become inter-connected, and eventually all the contour lines become represented as co-centred circles. The radial pressure distribution also changes with liquid level.

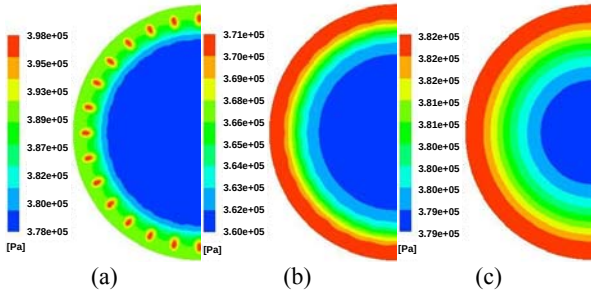

Figure 19: Pressure distribution on liquid surface for different liquid level: (a) 0.75 m; (b) 1m and (c) 2m below the tuyere centre level.

Tuyere Gas Flowrate

The mean pressure on the liquid surface increases with the gas flowrate to the power of 1.93 (Figure 20). The SPD also follows a similar trend.

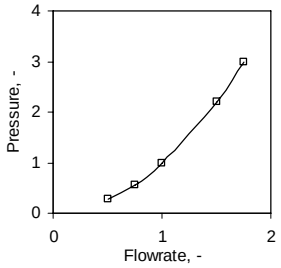

Figure 20: Liquid surface pressure versus tuyere gas flowrate (scaled relative to the base case).

Effect of Raceway

To examine the effect of the assumed raceway dimension, the size of raceway cavity or the entire raceway (including the fine coke region) has been scaled relative to a base case. Generally, the pressure difference on the liquid surface increases with increasing raceway size, as shown in Figure 21. The effect of a change in the entire raceway size is stronger than the change in cavity size alone. A local minimum in SPD appears, which probably (not investigated in this paper) represents the transition point in the importance of mean cavity pressure relative to the closeness of the raceway wall to the liquid surface when raceway size changes.

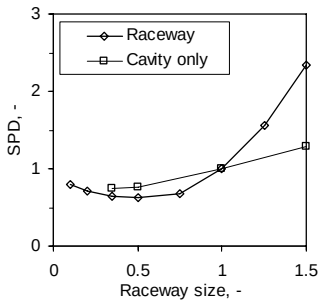

Figure 21: SPD versus raceway size (scaled relative to the base case). Liquid level: 1.5m below tuyere.

Worst Case Scenario

A specific 'worst case' scenario was investigated where the root position of a 'W'-shaped CZ is fixed at 2.5 m above the tuyere level, the deadman surface angle set at 45º, the deadman porosity set at 0.1 and the liquid level is varied. Under such conditions, the CZ nearly touches the deadman surface (Figure 22), so the gas-liquid interaction will be exaggerated compared with the base case. The SPD is high and depends strongly on the liquid level (
Figure **23**). When the liquid level is at the taphole level, the liquid surface pressure becomes more uniform. Nevertheless, integration of the surface pressure when the liquid surface is at the taphole level indicates that an extra slag residual of more than 0.6 m^3 could result from the liquid surface pressure variation. Although this amount seems to be quite small, the exact value is expected to be higher in a dynamic system during the tapping process, due to a higher pressure difference initially.

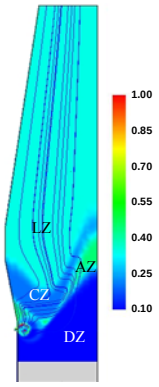

Figure 22: Porosity distribution and streamlines for a 'worst case' scenario.

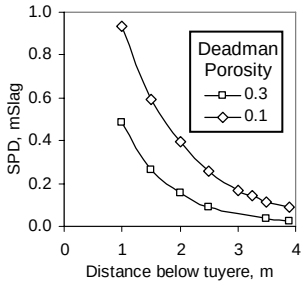

Figure 23: Effect of liquid level on SPD for a 'worst case' scenario.

CONCLUSIONS

Gas flow and pressure distribution on the liquid surface are calculated in a three-dimensional sector model of a blast furnace. The effects of several parameters are investigated systematically to provide a quantitative analysis concerning the extent of the liquid-gas interaction in the lower zone. It is found that the gas flow is sensitive to the assumed coke bed structure, such as the spatial distribution of mean porosity and particle size in the raceway, as well as the location of cohesive zone relative to the raceway.

It is shown that the gas flow creates a non-uniform pressure over the slag surface and this can cause this surface to deform. For the two types of cohesive zone considered, the 'W'-shaped cohesive zone tends to affect the liquid surface profile more than the 'inverted V'-shaped cohesive zone. Under normal operational conditions, the gas flow distribution is not significantly affected by the liquid level. The liquid surface pressure difference decreases as the liquid level drops.

ACKNOWLEDGEMENT

This work is supported by the Australian Research Council and BlueScope Steel.

REFERENCES

CASTRO, J.A., NOGAMI, H. and YAGI, J., (2002), "Three-dimensional multiphase mathematical modeling of the blast furnace based on the multifluid model", *ISIJ Int.*, **42**, 44-52.

CHEW, S.J., ZULLI, P. and YU, A.B., (2001), "Modelling of liquid flow in the blast furnace. Application in a comprehensive blast furnace model", *ISIJ Int.*, **41**, 1122-1130

DONG, X.F., PINSON, D., ZHANG, S.J., YUu, A.B., ZULLI, P., (2006), "Gas-powder flow in blast furnace with different shapes of cohesive zone", *Appl. Math. Modelling* (in press).

HE, Q., ZULLI, P, TANZIL, F., LEE, B., DUNNING, J. and EVANS, G., (2002), "Flow characteristics of a blast furnace taphole stream and its effects on trough refractory wear", *ISIJ Int.* **42**, 235-242.

ISIJ, Blast Furnace Phenomena and Modelling. Elsevier Applied Science, 1987.

MONDAL, S.S., SOM, S.K. and DASH, S.K., (2005), "Numerical predictions on the influences of the blast velocity, initial bed porosity and bed height on the shape and size of raceway zone in a blast furnace", *J. Phys D: Appl. Phys.*, **38**, 1301-1307.

NISHIOKA, K., MAEDA, T. and SHIMIZU, M., (2005), "A three-dimensional mathematical modelling of drainage behavior in blast furnace hearth", *ISIJ Int.*, **45** , 669-676.

NOGAMI, H., AUSTIN, P.R., YAGI, J. and YAMAGUCHI, K., (2004a), "Numerical investigation on effects of deadman structure and powder properties on gas and powder flows in lower part of blast furnace", *ISIJ Int.*, **44**, 500-509.

NOGAMI, H., YAMAOKA, H. and TAKATANI, K., (2004b), "Raceway design for the innovative blast furnace", *ISIJ Int.*, **44**, 2150-2158.

PANJKOVIC, V., TRUELOVE, J.S., ZULLI, P., (2002), "Numerical modelling of iron flow and heat transfer in blast furnace hearth", *Ironmaking and Steelmaking*, **29**, 390-400.

PINCZEWSKI, W.V. and TANZIL, W.B.U., (1981), "A numerical solution for the drainage of two-dimensional packed beds", *Chem. Eng. Sci.*, **36**, 1039-1043.

TANZIL, W.B.U., Blast Furnace Hearth Drainage, Ph.D. Thesis, University of New South Wales, 1985.

TATE, M, KUWANO, Y, SUZUKI, K, et al., (1972), "Observation of high-temperature region in an experimental blast-furnace by means of fiber-scope or bore-scope", *Trans. ISIJ*, **16**, 447-452.